minerals

MDPI

Article

Petrogenesis of the Early Cretaceous Tietonggou Diorite and Its Geological Implications

Guo Ye [1], Guangzhou Mao [1,2,3,*], Qinglin Xu [1], Zhengjiang Ding [3], Yanchao Han [1,4], Huiji Zhao [1,4] and Ying Shen [5]

[1] Shandong Key Laboratory of Depositional Mineralization & Sedimentary Minerals, College of Earth Sciences & Engineering, Shandong University of Science and Technology, Qingdao 266590, China; yeguo151@163.com (G.Y.); xql_618@163.com (Q.X.); 15605316566@163.com (Y.H.); 18660136058@163.com (H.Z.)
[2] Functional Laboratory of Marine Mineral Resources Evaluation and Detection Technology, Qingdao National Laboratory of Marine Science and Technology, Qingdao 266237, China
[3] Shandong Engineering Research Center of Application and Development of Big Data for Deep Gold Exploration, Weihai 264209, China; ytdzhj@126.com
[4] Shandong Geo-Surveying & Mapping Institute, Ji'nan 250003, China
[5] Shandong Institute of Geological Sciences, Ji'nan 250013, China; shenyingdky@shandong.cn
* Correspondence: gzmaonjunwu@163.com

Abstract: The Tietonggou pluton is mainly composed of gabbroic diorite and diorite. The petrology, zircon U-Pb age, and geochemistry of the Tietonggou diorite have been studied to determine its petrogenesis and metallogenic significance. The diorite samples have 56–58 wt% SiO_2 and 11–14 wt% Al_2O_3 and are peraluminous and sodic (Na_2O/K_2O = 1.29–2.07). All the samples are enriched in light rare earth elements (LREEs) and large-ion lithophile elements (LILEs; e.g., Rb, Ba, and Sr) but depleted in heavy rare earth elements (HREEs) and high field strength elements (HFSEs; e.g., Zr, Nb, and Ta), suggesting subduction-related affinities. The rocks have narrow ranges of $(^{206}Pb/^{204}Pb)_t$ (18.5–19.0), $(^{207}Pb/^{204}Pb)_t$ (15.71–15.75), and $(^{208}Pb/^{204}Pb)_t$ (38.4–39.0) ratios, respectively. Zircons from the Tietonggou diorite yielded a weighted average U-Pb age of 132.86 ± 0.92 Ma (MSWD = 0.48), whilst those from the nearby Laowa diorite yielded 129.72 ± 0.61 Ma (MSWD = 1.05). This suggests that the rocks represent Early Cretaceous plutons, coeval with the peak lithospheric thinning in eastern North China Craton (NCC). The magma likely originated from partial melting of the enriched lithospheric mantle and was contaminated by ancient lower NCC crustal materials. Our study clarifies the tectonic background of the Tietonggou pluton and provides support for the study of the genesis of Fe–skarn deposits in western Shandong.

Keywords: zircon U-Pb dating; geochemistry; Mesozoic; Tietonggou pluton; western Shandong

Citation: Ye, G.; Mao, G.; Xu, Q.; Ding, Z.; Han, Y.; Zhao, H.; Shen, Y. Petrogenesis of the Early Cretaceous Tietonggou Diorite and Its Geological Implications. *Minerals* **2024**, *14*, 390. https://doi.org/10.3390/min14040390

Academic Editor: Paul Alexandre

Received: 28 February 2024
Revised: 3 April 2024
Accepted: 4 April 2024
Published: 9 April 2024

1. Introduction

Since the Triassic continental collision between the North China Craton (NCC) and Yangtze Craton, NCC has undergone lithospheric thinning and large-scale magmatism; post-collision magmatism produced several Triassic plutons on the southern and eastern margins of the NCC [1]. Western Shandong is located in the southeastern NCC, west of the Yishu fault (a section of the crustal Tanlu fault zone) and adjacent to the Sulu–Dabie UHP belt (Figure 1a). There are many Fe–skarn deposits closely associated with these Mesozoic plutons. As one of the four major Fe–skarn deposit concentration areas in China, the western Shandong shows extensive Mesozoic magmatism and mineralization, making it an important area for studying the NCC formation and evolution [1–6], especially in terms of crust–mantle interactions [7–11]. Tietonggou is one of the two Fe–skarn deposits related to diorite in western Shandong, which are mainly produced in the contact zone between intrusive bodies and Cambrian–Ordovician, with cumulative Fe reserves of 2.11 million tons. Compared with the Jiaodong Peninsula, there are far fewer Mesozoic magmatic rock

outcrops in western Shandong, and the Tietonggou pluton is one of them; their ages were reported as 184.7–180.1 Ma, 133 ± 6 Ma, 120 Ma, etc. [3,4,12].

In recent years, many petrological, geochronological, and geochemical studies have been conducted regarding Mesozoic Fe–skarn deposits and related intermediate-basic intrusive rocks in western Shandong [1–17]. The Tietonggou pluton was considered to have originated from the partial melting of pure peridotite in the upper mantle with continental crust input [13–16], yet there are different views on the crustal input: (1) Yangtze plate materials introduced during its Triassic subduction and collision [15,16]; (2) Archean North China crustal material sunk into the mantle during lithospheric delamination [17]; (3) Paleo-Pacific materials introduced during its subduction beneath North China [13].

Previous researchers focused on the Mesozoic pluton and Fe–skarn deposits in the whole western Shandong area and the lack of special research on the Tietonggou pluton. They have different opinions on the source of crust input in the metallogenic material of the Tietonggou pluton, and there are no reports on the accurate metallogenic age of the Tietonggou pluton.

In this study, we carried out analyses in petrology, whole-rock geochemistry, and zircon U-Pb geochronology on the Tietonggou pluton. The precise metallogenic age of the Tietonggou rock mass was obtained, and the possible material sources were analyzed. We discuss its petrogenesis and regional tectonic significance in order to clarify the tectonic background of the Tietonggou pluton and point out the targets for iron ore prospecting. The precise U/Pb zircon ages of the plutonic rocks in China can be used to establish geodynamics models for future studies.

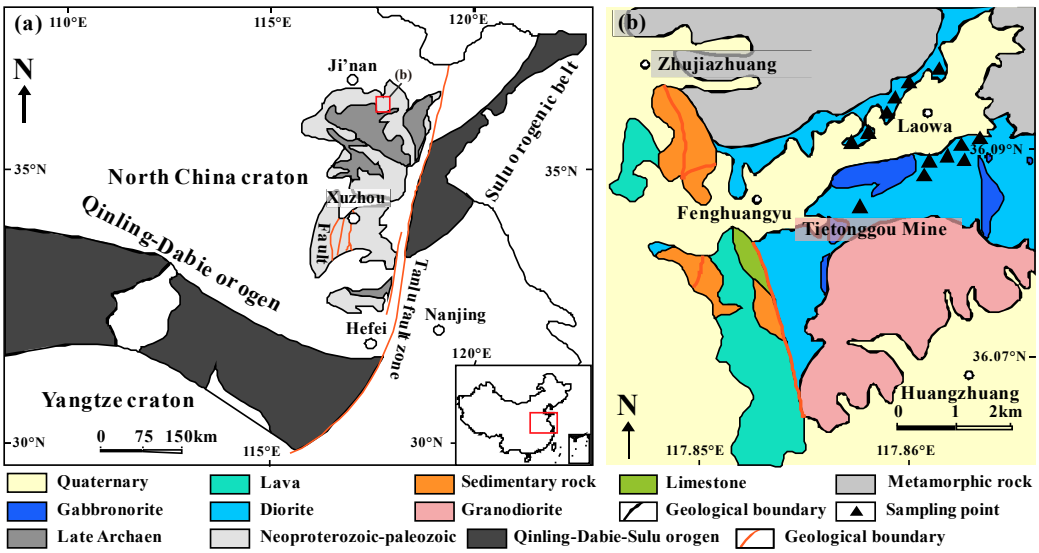

Figure 1. (**a**) Regional geological maps of western Shandong (modified after [18,19]); (**b**) Tietonggou area (modified after [20,21]).

2. Geological Setting and Petrography

Western Shandong was tectonically affected by the Lüliang, Caledonian, Hercynian, Indosinian, and Yanshanian orogenic events, forming a WNW-NW-trending tectonic framework. Mesozoic intrusive rocks are well-developed in western Shandong [18], as represented by the Laiwu and Ji'nan intrusive complexes (Figure 1a). Local stratigraphy comprises mainly the Ordovician Majiagou Group and the Carboniferous–Permian Yuemengou–Taiyuan groups. There are three major sets of faults (NW-, NE-, and EW-trending). Local magmatic rocks are dominated by Yanshanian (Jurassic–Cretaceous) intermediate plutonic rocks (notably the Tietonggou pluton) and minor mafic and felsic rocks (Figure 1b). The magmatic rock emplacement is locally fault-controlled, and the wallrocks include mainly Ordovician and Triassic marble [22].

The Tietonggou pluton comprises mainly meladiorite and diorite, which were mainly developed along the intrusive contact with the Ordovician Majiagou Group and the Carboniferous–Permian Yuemengou–Taiyuan groups. Samples LW1-LW12 were taken from Laowa village (where the Tietonggou pluton is exposed). The intrusive contact with the altered wallrocks is distinct in the mine (Figure 2a). The diorite is grayish-black (Figure 2c) and contains mafic microgranular enclaves (peridotite, a few cm in dimension). These inclusions contain 60%–65% olivine, 10%–15% orthopyroxene, and accessory minerals such as apatite (Figure 2d).

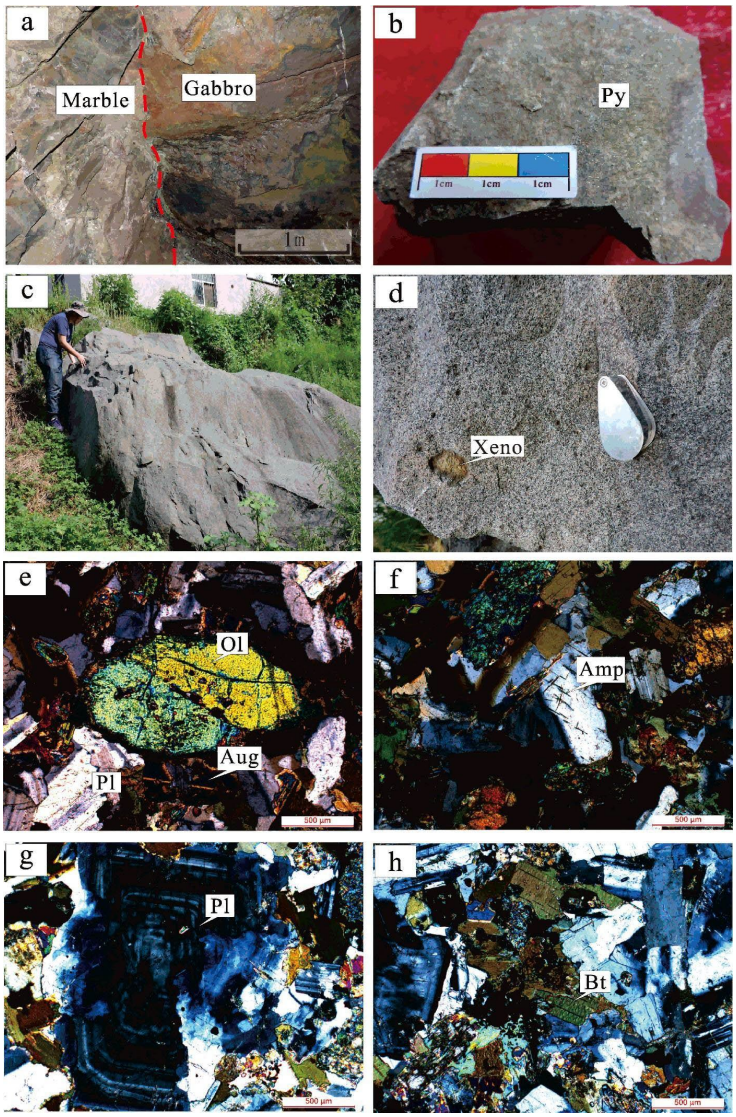

Figure 2. Field photos and thin-section microphotographs of the Tietonggou pluton: (**a**) intrusive contact between diorite and marble; (**b**) meladiorite; (**c**) Laowa diorite; (**d**) diorite with augite xenoliths; (**e**) spindle olivine; (**f**) amphibole; (**g**) oscillatory-zoned plagioclase; (**h**) biotite. Py—Pyrite; Ol—olivine; Aug—augite; Pl—plagioclase; Amp—amphibole; Bt—biotite.

Under the microscope, the olivine is granular and cracked. The pyroxene is euhedral to subhedral granular and ranges from coarse- to fine-grained (Figure 2e). The hornblende is greenish and unevenly distributed (Figure 2f). Plagioclase is euhedral–subhedral tabular, and some crystals are oscillatory-zoned (Figure 2g), whilst biotite is flaky, dark brown, and of different sizes (Figure 2h). Opaque minerals include mainly magnetite.

3. Methods

In this study, a total of twelve samples were collected, including 2 meladiorite and 10 diorite. Meladiorite is the transition from diorite to gabbro. The dark minerals are mainly clinopyroxene (25%), containing a small amount of amphibole and orthopyroxene (about 5%). All the samples were collected from fresh outcrops of the Tietonggou pluton (Figure 2). Whole-rock major oxides, trace elements analyses, Pb isotope analysis, and zircon U-Pb dating were used to determine the tectonic implications (Figure 3).

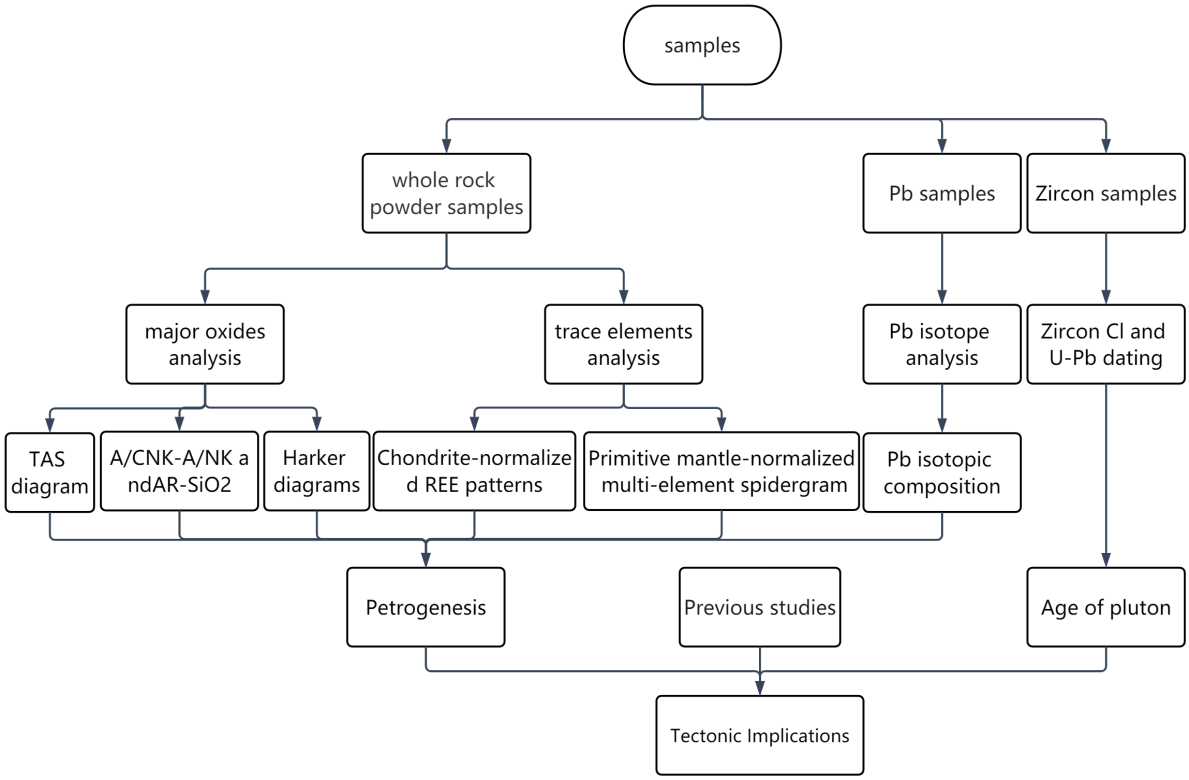

Figure 3. Methods flow chart.

3.1. Whole-Rock Major Oxides and Trace Elements Analyses

The analyses were carried out at the Institute of Geochemistry, Chinese Academy of Sciences (IGCAS) with an Agilent 5110 ICP-OES (Agilent Technologies, Santa Clara, CA, USA). For each sample, 0.0400 g powder was weighed into a Teflon cup, and 0.5 mL HNO_3 and 1 mL HF were successively added, sealed, and heated in an oven at 200 °C for 12 h. The sample solution was then dried at 150 °C on an electric heating plate and then redigested with 5 mL 12% (*v*/*v*) HNO_3 at 150 °C for 5 h. The solution was then diluted and analyzed [23]. The analysis accuracy of major oxides and trace elements is less than ±1 and ±5.

3.2. Whole-Rock Pb Isotope Analysis

Wole-rock Pb isotopic composition was measured out in the IGCAS with a Neptune plus MC-ICP-MS (Thermo Fisher Scientific, Dreieich, Germany). The rock powder was placed in the polytetrafluoroethylene sample cartridge, and 0.5 mL concentrated HNO_3 and 1.0 mL concentrated HCl were added. The sample dissolving bomb was heated (195 °C) in an oven for three days to ensure complete digestion. The solution was then evaporated on an electric heating plate and redissolved in 1.5 mL of HBr (0.2 mol/L) and HNO_3 (0.5 mol/L). Detailed procedures were described by [24].

3.3. Zircon U-Pb Dating

Zircon grains were separated by conventional magnetic separation and heavy liquid techniques. Optical microscopic observation, scanning electron microscope (SEM) cathodoluminescence (CL) imaging, and analysis spot selection of zircons were completed at the Beijing Zircon Navigation Technology Co. Ltd., and the zircon U-Pb dating was carried out at the State Key Laboratory of Continental Dynamics of Northwestern University with an Agilent 7500a ICP-MS (Agilent Technologies, Santa Clara, CA, USA). The laser ablation used helium as the carrier gas, 20 μm spot size, 0.032–0.036 J/cm^2 energy density, and 10 Hz repetition rate. The calibration was performed with standard zircon 91,500 and GJ-1 [25–27]. ISOPLOT 3.0 software was used to process the data results and calculate the age. Detailed procedures were as described by [28].

4. Results

4.1. Whole-Rock Geochemistry

In our study, 12 rock samples (2 meladiorite and 10 diorite) were analyzed for their major oxides and trace element compositions, which are listed in Table 1, respectively. The rock samples have SiO_2 = 56–58 wt% (avg. 57.6 wt%), Al_2O_3 = 11.31–14.15 wt% (avg. 13.3 wt%), Na_2O = 2.6–3.5 wt%, K_2O = 1.63–2.55 wt%, Na_2O+K_2O = 4.50–5.99 wt%, and Na_2O/K_2O = 1.29–2.07. In the total alkali silica (TAS) diagram (Figure 4), the samples fall within the meladiorite–diorite field, and most of the samples are subalkaline. The rocks have MgO = 7.14–10.43 wt%, CaO = 5.99–7.29 wt%, and a loss on ignition (LOI) = 0.28–0.88 wt%. Na_2O, TiO_2, and K_2O contents increase with increasing SiO_2 content, while Fe_2O_3, CaO, and MgO decrease (Figure 5). In the A/CNK-A/NK diagram (Figure 6a), the meladiorite and diorite samples fall into the metaluminous and peraluminous fields, respectively. In the SiO_2-AR diagram (Figure 6b), all Tietonggou samples are assigned as calc-alkaline.

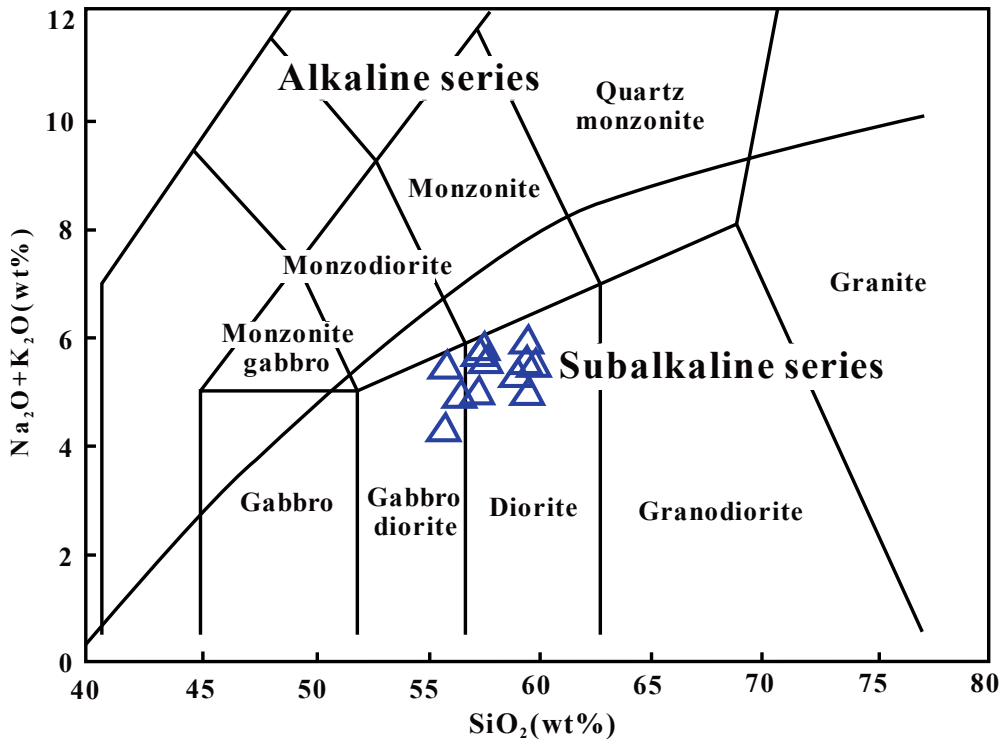

Figure 4. TAS diagram for the Tietonggou samples [29,30].

Table 1. Major oxides composition and trace elements composition for the Tietonggou diorite and meladiorite samples.

Major Oxides in wt%	Diorite (n = 10)			Meladiorite		Major Oxides in wt%	Diorite (n = 10)			Meladiorite	
	Min	Mean	Max	LW-5	LW-6		Min	Mean	Max	LW-5	LW-6
Na_2O	2.94	3.28	3.46	2.57	3.49	MnO	0.11	0.11	0.12	0.13	0.11
MgO	7.14	7.83	8.83	10.43	7.58	Fe_2O_3	6.67	7.11	7.59	8.21	7.16
Al_2O_3	12.23	13.4	14.15	11.31	14.11	LOI	0.28	0.51	0.79	0.88	0.58
SiO_2	56.4	57.6	58.38	56.17	56.91	Total	99.15	99.4	99.64	99.77	99.3
P_2O_5	0.14	0.19	0.21	0.12	0.21	$K_2O + Na_2O$	5.02	5.55	5.99	4.5	5.54
K_2O	1.63	2.27	2.55	1.92	2.05	A/NK	2.33	2.42	2.66	2.51	2.55
CaO	5.99	6.41	7.2	7.29	6.43	A/CNK	1.02	1.12	1.16	0.96	1.18
TiO_2	0.62	0.67	0.72	0.73	0.68	Na_2O/K_2O	1.29	1.46	2.07	1.34	1.7
Trace and Rare Earth Elements in ppm	**Diorite (n = 10)**			**Meladiorite**		**Trace and Rare Earth Elements in ppm**	**Diorite (n = 10)**			**Meladiorite**	
	Min	**Mean**	**Max**	**LW-5**	**LW-6**		**Min**	**Mean**	**Max**	**LW-5**	**LW-6**
Li	19.3	21.83	24.8	23.6	21.3	Ho	0.47	0.501	0.52	0.55	0.45
Be	1.53	1.643	1.75	1.5	1.54	Er	1.27	1.348	1.42	1.46	1.2
Sc	17.9	19.56	22.5	25.9	18.2	Tm	0.18	0.194	0.2	0.21	0.17
Ti	3705	3907.6	4258	4356	3912	Yb	1.15	1.214	1.3	1.32	1.08
V	139	147.8	164	174	146	Lu	0.17	0.178	0.19	0.19	0.16
Cr	587	676.9	857	922	651	Hf	2.94	3.492	5.05	2.56	3.07
Mn	813	858.5	919	1033	852	Ta	0.39	0.447	0.5	0.42	0.42
Co	27.4	29.8	33.2	39.3	28.8	Pb	14.5	16.95	18.8	12.7	16.3
Ni	161	178.7	207	247	170	Th	5.34	6.564	7.92	6.24	6.26
Cu	2.07	36.131	178	205	51.4	U	1.42	1.878	2.13	1.71	1.65
Zn	70.9	79.08	82.5	83	76.3	Nb/Ta	14.44	15.792	16.82	14.27	14.76
Ga	17.7	18.75	19.7	16.4	18.4	Rb/Sr	0.1	0.13	0.16	0.16	0.11
As	6.95	7.392	7.99	6.76	6.24	Ba/Rb	9.56	12.183	14.08	12.48	13.6
Se	0.54	0.649	0.83	0.61	0.47	Zr/Hf	35.42	37.659	39.14	34.82	37.51
Rb	51.6	63.1	68.2	59.6	56.8	La/Sm	4.51	5.299	5.67	4.25	5.71
Sr	419	483.9	525	382	523	Zr/Nb	14.79	18.869	28.02	15.03	18.62
Y	12.4	13.45	14	14.7	12.1	Ta/La	0.02	0.021	0.03	0.02	0.02
Zr	104	132	198	89.2	115	Ce/Pb	2.32	2.547	2.84	2.94	2.57
Nb	5.67	7.038	7.61	5.94	6.18	Hf/Sm	0.71	0.862	1.22	0.62	0.82
Mo	3.85	4.656	5.51	3.76	4.16	Nb/La	0.27	0.329	0.39	0.34	0.29
Sn	1.24	1.34	1.47	1.22	1.4	Th/La	0.26	0.305	0.34	0.35	0.29
Cs	4.07	4.58	5.12	3.69	4.05	Y/Ho	26.26	26.807	27.83	26.69	26.63
Ba	493	771.2	840	743	773	Co/Ni	0.16	0.168	0.17	0.16	0.17
La	18.5	21.46	23.2	17.6	21.3	$(La/Yb)_N$	10.13	11.954	12.84	8.99	13.3
Ce	38.2	43.01	45.7	37.5	42	∑REEs	95.08	104.15	109.48	94.29	100.25
Pr	4.46	4.901	5.21	4.4	4.63	∑LREEs	85.09	94.319	99.69	83.6	91.33
Nd	18.6	19.83	20.6	18.9	18.6	∑HREEs	9.23	9.832	10.24	10.69	8.91
Sm	3.74	4.053	4.15	4.15	3.73	LREEs/HREEs	8.51	9.6	10.19	7.82	10.25
Eu	0.98	1.068	1.13	1.04	1.14	$(Gd/Yb)_N$	2.11	2.205	2.28	2.17	2.27
Gd	3.07	3.312	3.39	3.56	3.03	$(La/Sm)_N$	2.84	3.333	3.56	2.67	3.59
Tb	0.44	0.473	0.49	0.51	0.43	δCe	1	1.01	1.02	1.02	1.02
Dy	2.47	2.615	2.73	2.89	2.39	δEu	0.81	0.891	0.99	0.83	1.03

LOI: loss on ignition.

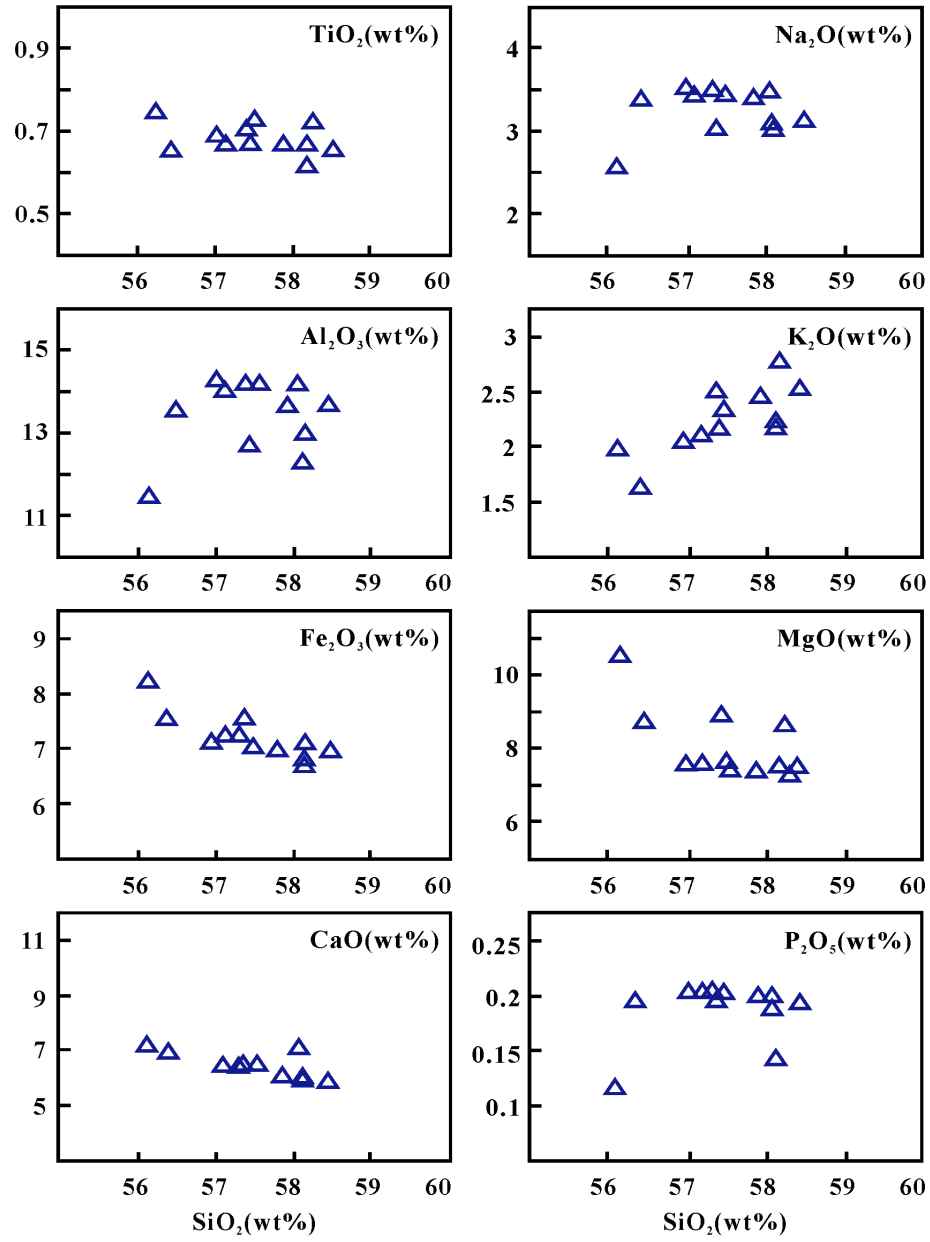

Figure 5. Harker diagrams for the Tietonggou meladiorite and diorite samples.

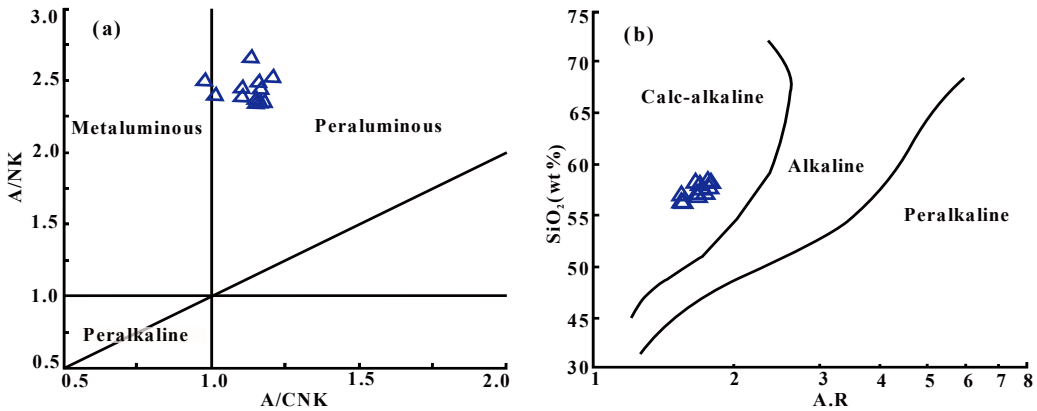

Figure 6. (**a**) A/CNK-A/NK [31] and (**b**) AR-SiO_2 [32] plots for the Tietonggou meladiorite and diorite samples. AR: Alkalinity ratio.

The total REE contents (∑REEs) for the Tietonggou samples are 94.29–109.48 ppm, among which the ∑LREEs = 83.60–99.69 ppm and ∑HREEs = 8.91–10.69 ppm, and the $(La/Yb)_N$ = 8.99–13.30. The rocks have weakly negative Eu anomalies (δEu = 0.81–1.03) and no discernible Ce anomalies (δCe = 1.00–1.02). The chondrite-normalized REE patterns show LREE enrichments and HREE depletions (Figure 7). In the primitive-mantle normalized multi-element spidergram (Figure 8), the rock samples are enriched in large ion lithophile elements (LILEs, e.g., Rb, Ba, Sr) but depleted in high field strength elements (HFSEs, e.g., Zr, Nb, Ta), resembling typical subduction-related arc magmatic rocks [33,34].

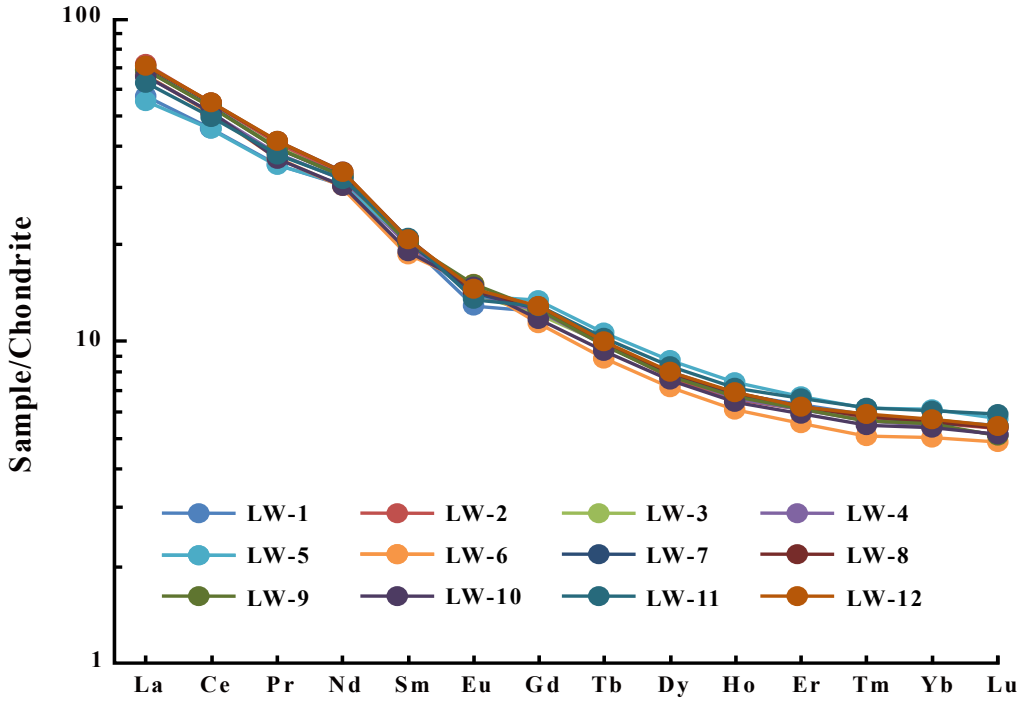

Figure 7. Chondrite-normalized REE patterns for the Tietonggou meladiorite and diorite samples [35].

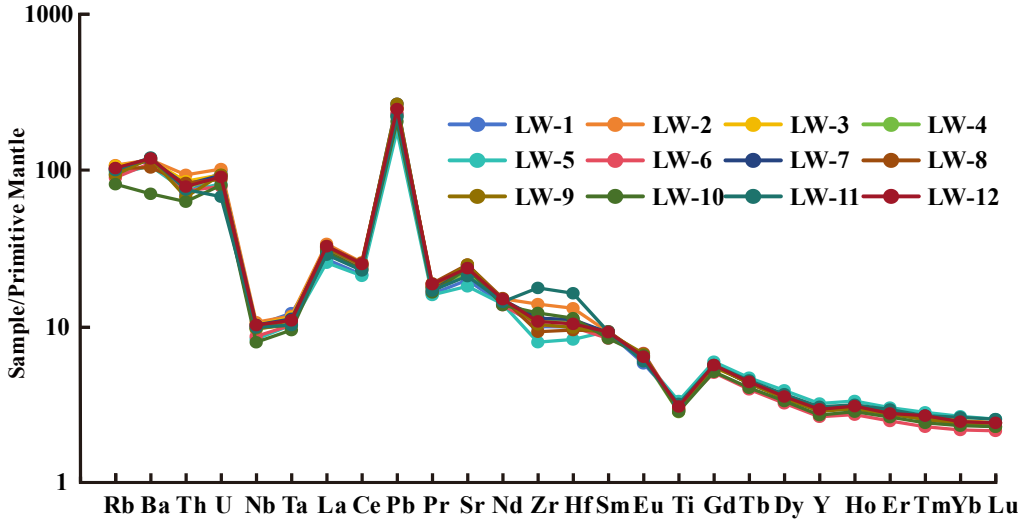

Figure 8. Primitive mantle-normalized multi-element spidergram for the Tietonggou meladiorite and diorite samples [36].

4.2. Pb Isotope Characteristics

The Pb isotope analysis results for the Tietongou diorite are listed in Table 2. The samples have $(^{206}Pb/^{204}Pb)_t$, $(^{207}Pb/^{204}Pb)_t$, and $(^{208}Pb/^{204}Pb)_t$ of 17.89–17.96, 15.48–15.50,

and 37.90–37.95, respectively. The initial Pb isotope data of the samples fall between the Tietonggou pyroxene diorite and Shangyu pyroxene diorite in western Shandong [37,38]. In the Pb isotopic composition diagram (Figure 9), the samples of the Tietonggou pluton are projected within the range of Mesozoic mafic rocks in the North China Craton and the Yangtze Craton (Figure 8), indicating that the magma source of the Tietonggou pluton is closely related to the Yangtze Craton [38,39].

Table 2. Whole-rock Pb isotope compositions for the Tietonggou meladiorite and diorite samples.

Sample No.	$^{208}Pb/^{204}Pb$	1σ	$^{207}Pb/^{204}Pb$	1σ	$^{206}Pb/^{204}Pb$	1σ	Pb (ppm)	Th (ppm)	U (ppm)	Age (Ma)	$(^{208}Pb/^{204}Pb)_t$	$(^{207}Pb/^{204}Pb)_t$	$(^{206}Pb/^{204}Pb)_t$
LW-1	38.0940	0.0013	15.4946	0.0004	18.0561	0.0003	16.1	5.95	2.07	129.7	37.9419	15.4867	17.8946
LW-2	38.1111	0.0013	15.5054	0.0004	18.1133	0.0003	17.6	7.92	2.13	129.7	37.9260	15.4980	17.9612
LW-3	38.0843	0.0017	15.4955	0.0005	18.0610	0.0004	17.4	7.21	1.96	129.7	37.9144	15.4886	17.9200
LW-4	38.0731	0.0015	15.4901	0.0005	18.0505	0.0004	15.6	6.57	1.88	129.7	37.9002	15.4827	17.8993
LW-5	38.1393	0.0020	15.5033	0.0006	18.1078	0.0005	12.7	6.24	1.71	129.7	37.9382	15.4951	17.9391
LW-6	38.1058	0.0014	15.5039	0.0004	18.0607	0.0004	16.3	6.26	1.65	129.7	37.9481	15.4977	17.9338

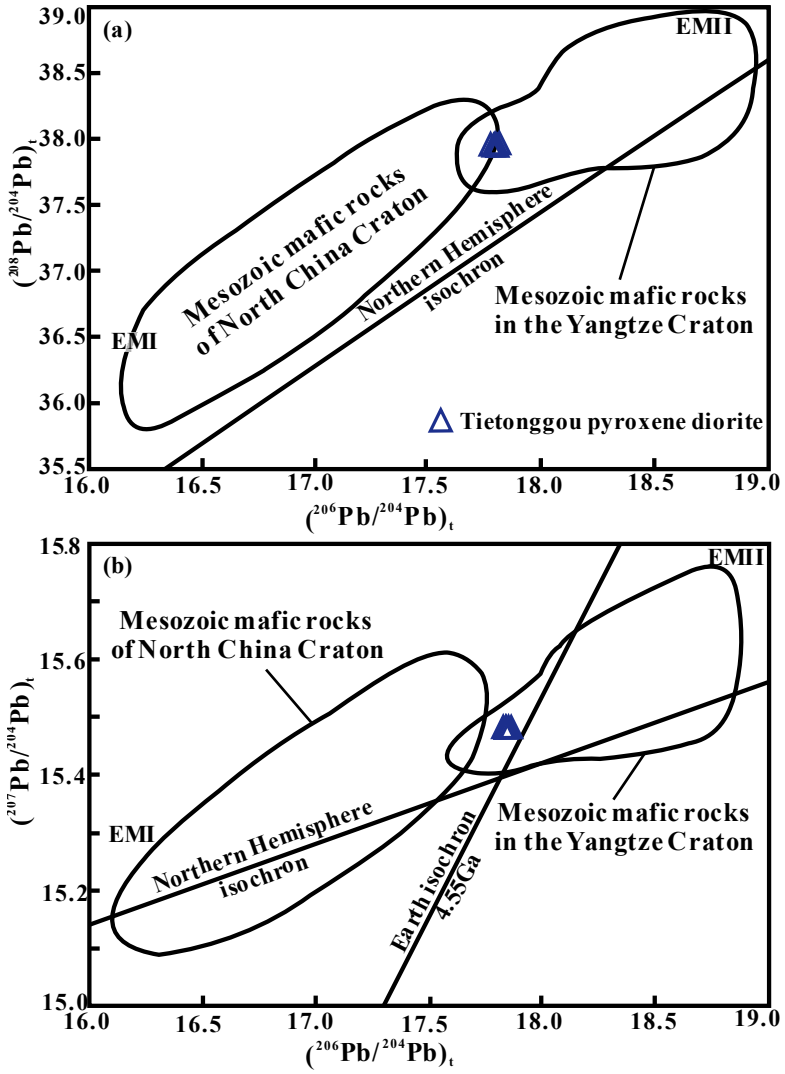

Figure 9. (**a**)$^{208}Pb/^{204}Pb$ versus $^{206}Pb/^{204}Pb$ diagram and (**b**) $^{207}Pb/^{204}Pb$ versus $^{206}Pb/^{204}Pb$ diagram for the Tietonggou meladiorite and diorite samples [40]. Data source: Mesozoic mafic rocks of North China Craton [38]; Mesozoic mafic rocks [38,39]; Northern Hemisphere reference line [41]; Earth isochron [42].

4.3. Zircon U-Pb Geochronology

For the present study, 23 zircons from the Tietonggou diorite (in the mine) and 27 zircons from the Laowa diorite were U-Pb dated. The zircons are transparent to translucent and mostly short to long columnar. Many zircons show core-rim texture (Figure 10). The zircons have Th/U > 0.4, resembling typical magmatic zircons [42] (Table 3). All analysis spots fall on or near the concordia, yielding a weighted average zircon age of 132.86 ± 0.92 Ma (MSWD = 0.48) for the Tietonggou pluton and 129.72 ± 0.61 Ma (MSWD = 1.05) for the Laowa pluton (Figure 11), suggesting an Early Cretaceous pluton.

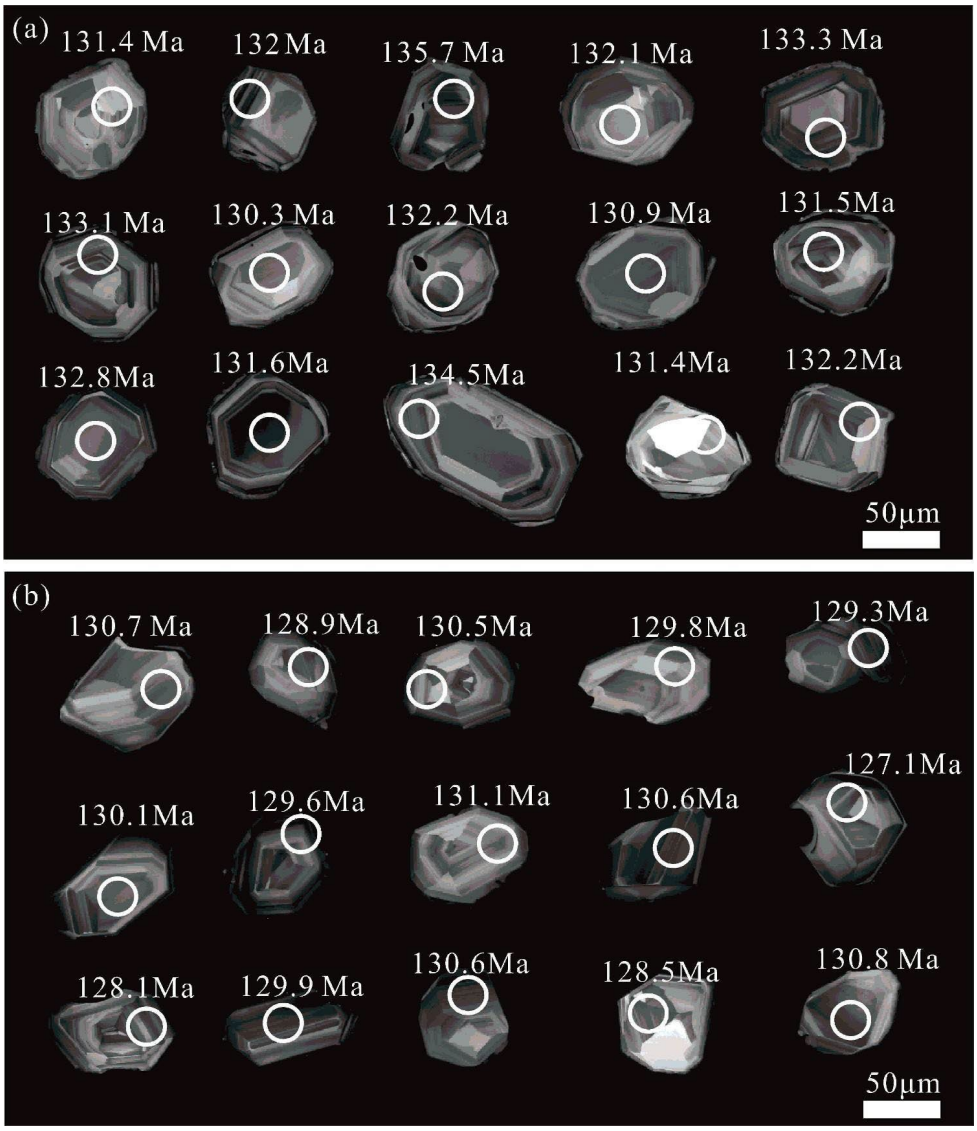

Figure 10. Representative zircon CL images and U-Pb ages for the Tietonggou (**a**) and Laowa (**b**) diorite samples.

Table 3. LA-ICP-MS zircon U-Pb dating results of the Tietonggou (TTGN) and Laowa (LW) diorite samples.

Sample No.	^{232}Th	^{238}U	Th/U	Isotopic Ratio						Isotopic Age	
	(ppm)	(ppm)		Pb^{207}/Pb^{206}	1sigma	Pb^{207}/U^{235}	1σ	Pb^{206}/U^{238}	1σ	Pb^{206}/U^{238}	1σ
91500				0.07427	0.0024	1.829	0.049	0.179	0.0023	1059.2	12.78
GJ-1				0.06161	0.0018	0.841	0.02	0.099	0.0012	608.5	7
TTG-Z1	61.48	115.97	0.53	0.0497	0.0051	0.141	0.014	0.021	0.0004	131.4	11.98
TTG-Z2	82.14	150.1	0.55	0.04865	0.0038	0.139	0.01	0.021	0.0003	132	8.32
TTG-Z3	110.77	230.75	0.48	0.04997	0.0034	0.147	0.01	0.021	0.0003	135.7	8.2
91500				0.07661	0.0023	1.892	0.047	0.179	0.0023	1061.9	12.71
TTG-Z4	187.35	161.64	1.16	0.04916	0.0047	0.14	0.013	0.021	0.0004	132.1	7.23
TTG-Z5	123.2	188.38	0.65	0.0496	0.004	0.143	0.011	0.021	0.0004	133.3	8.34
TTG-Z6	115.02	198.11	0.58	0.04883	0.0034	0.14	0.009	0.021	0.0003	133.1	7.82
TTG-Z7	114.57	154.57	0.74	0.05016	0.005	0.141	0.014	0.02	0.0004	130.3	9.63
91500				0.07263	0.0023	1.807	0.048	0.18	0.0023	1069.3	12.78
GJ-1				0.06131	0.0018	0.826	0.019	0.098	0.0012	601.1	6.78
TTG-Z8	267.55	365.62	0.73	0.04947	0.0026	0.141	0.007	0.021	0.0003	132.2	4.8
TTG-Z9	110.03	179.11	0.61	0.05195	0.0059	0.147	0.016	0.021	0.0005	130.9	12.88
TTG-Z10	386.74	276.92	1.4	0.0493	0.0027	0.14	0.007	0.021	0.0003	131.5	3.61
TTG-Z11	384.12	231.61	1.66	0.04884	0.0032	0.14	0.009	0.021	0.0003	132.8	3.92
TTG-Z12	84.14	138.04	0.61	0.05177	0.0046	0.147	0.013	0.021	0.0004	131.6	9.73
TTG-Z13	67.1	156.02	0.43	0.04999	0.0043	0.145	0.012	0.021	0.0004	134.5	11.63
TTG-Z14	252.55	212.17	1.19	0.04971	0.004	0.141	0.011	0.021	0.0004	131.4	5.6
TTG-Z15	134.69	144.47	0.93	0.04944	0.0041	0.141	0.011	0.021	0.0004	132.2	6.9
TTG-Z16	143.1	206.13	0.69	0.05001	0.0038	0.146	0.01	0.021	0.0004	134.7	7.76
TTG-Z17	128	222.33	0.58	0.0496	0.0031	0.143	0.008	0.021	0.0003	133.4	6.8
91500				0.07613	0.0023	1.878	0.048	0.179	0.0023	1060.8	12.51
GJ-1				0.0597	0.0018	0.808	0.02	0.098	0.0012	603.8	6.84
TTG-Z18	69.01	126.7	0.55	0.05092	0.0041	0.149	0.012	0.021	0.0004	135.3	9.98
TTG-Z19	493.64	468.57	1.05	0.05086	0.004	0.143	0.011	0.02	0.0004	130.5	6.72
TTG-Z20	201.77	318.28	0.63	0.04881	0.0031	0.14	0.008	0.021	0.0003	133.2	6.67
TTG-Z21	747.54	357.87	2.09	0.04974	0.0029	0.145	0.008	0.021	0.0003	134.9	3.25
91500				0.07687	0.0024	1.902	0.049	0.179	0.0023	1063.7	12.58
TTG-Z22	70.4	142.06	0.5	0.04897	0.0046	0.143	0.013	0.021	0.0004	135.5	11.93
TTG-Z23	219.24	238.42	0.92	0.04875	0.0032	0.139	0.009	0.021	0.0003	131.7	5.62
91500				0.07306	0.0023	1.801	0.046	0.179	0.0023	1060.2	12.47
GJ-1				0.05931	0.0018	0.804	0.019	0.098	0.0012	604.5	6.83
91500				0.07252	0.002	1.792	0.045	0.179	0.0017	1062.8	9.35
GJ-1				0.05931	0.0014	0.801	0.017	0.098	0.0008	602.8	4.43
LW-Z1	379.47	273.91	1.39	0.05012	0.0027	0.142	0.007	0.02	0.0002	130.7	1.52
LW-Z2	190.8	178.01	1.07	0.04799	0.0031	0.134	0.009	0.02	0.0002	128.9	1.54
LW-Z3	541.49	367.17	1.48	0.04896	0.0021	0.138	0.006	0.02	0.0002	130.5	1.29
LW-Z4	1213.2	663.15	1.83	0.04857	0.0022	0.136	0.006	0.02	0.0002	129.8	1.34
LW-Z5	116.05	171.04	0.68	0.04752	0.0035	0.133	0.01	0.02	0.0003	129.3	1.77
91500				0.07675	0.0019	1.895	0.045	0.179	0.0017	1061.9	9.01
LW-Z6	300.65	286.17	1.05	0.04921	0.0026	0.138	0.007	0.02	0.0002	130.1	1.43
LW-Z7	580.1	348.18	1.67	0.04802	0.0028	0.134	0.008	0.02	0.0003	129.6	1.56
LW-Z8	114.86	175.5	0.65	0.04828	0.0035	0.137	0.01	0.021	0.0003	131.1	1.75
LW-Z9	378.59	324.78	1.17	0.04764	0.0025	0.134	0.007	0.02	0.0002	130.6	1.43
LW-Z10	427.37	296.14	1.44	0.04889	0.0031	0.134	0.008	0.02	0.0003	127.1	1.67
91500				0.07592	0.0019	1.875	0.043	0.179	0.0016	1062	8.9
GJ-1				0.0609	0.0014	0.824	0.017	0.098	0.0008	603.1	4.39
LW-Z11	249.85	313.26	0.8	0.04937	0.0023	0.137	0.006	0.02	0.0002	128.1	1.26
LW-Z12	396.86	323.93	1.23	0.048	0.0022	0.135	0.006	0.02	0.0002	129.9	1.26
LW-Z13	169.18	141.85	1.19	0.05191	0.0054	0.146	0.015	0.02	0.0004	130.6	2.57
LW-Z14	168.21	199.63	0.84	0.05083	0.0061	0.141	0.016	0.02	0.0005	128.5	3.22
LW-Z15	337.79	256.87	1.32	0.04856	0.0025	0.137	0.007	0.02	0.0002	130.8	1.45
LW-Z16	550.37	415.21	1.33	0.04971	0.0022	0.138	0.006	0.02	0.0002	128.8	1.3
91500				0.07414	0.0021	1.827	0.048	0.179	0.0018	1059.6	9.75
LW-Z17	354.96	280.68	1.27	0.04856	0.0025	0.134	0.007	0.02	0.0002	127.7	1.31
LW-Z18	259.38	224.88	1.15	0.04946	0.0036	0.137	0.01	0.02	0.0003	128.2	1.96
LW-Z19	723.6	420.6	1.72	0.04828	0.0028	0.132	0.007	0.02	0.0002	126.2	1.52
LW-Z20	219.32	186.64	1.18	0.04913	0.0035	0.14	0.010	0.021	0.0003	131.6	1.8
91500				0.07549	0.002	1.873	0.047	0.18	0.0017	1066.5	9.29
GJ-1				0.05987	0.0014	0.806	0.017	0.098	0.0007	600.2	4.37
LW-Z21	258.85	222.75	1.16	0.04843	0.0042	0.14	0.012	0.021	0.0004	133.3	2.3
LW-Z22	488.92	389.94	1.25	0.04838	0.0045	0.138	0.012	0.021	0.0004	131.5	2.59
LW-Z23	241.98	192.34	1.26	0.04953	0.0029	0.143	0.008	0.021	0.0003	133.5	1.58
LW-Z24	256.51	206.45	1.24	0.04852	0.0033	0.137	0.009	0.021	0.0003	130.8	1.68
LW-Z25	199.1	160.92	1.24	0.05135	0.0045	0.146	0.012	0.021	0.0004	131.1	2.19
91500				0.07487	0.0019	1.857	0.045	0.180	0.0017	1065.7	9.09
LW-Z26	174.94	198.49	0.88	0.05072	0.0046	0.143	0.013	0.02	0.0004	130.6	2.44
LW-Z27	165.69	225.14	0.74	0.04954	0.0039	0.137	0.011	0.02	0.0003	128.1	2.04
91500				0.07402	0.0020	1.822	0.045	0.178	0.0017	1058.2	9.12
GJ-1				0.0601	0.0015	0.819	0.019	0.099	0.0008	606.7	4.67

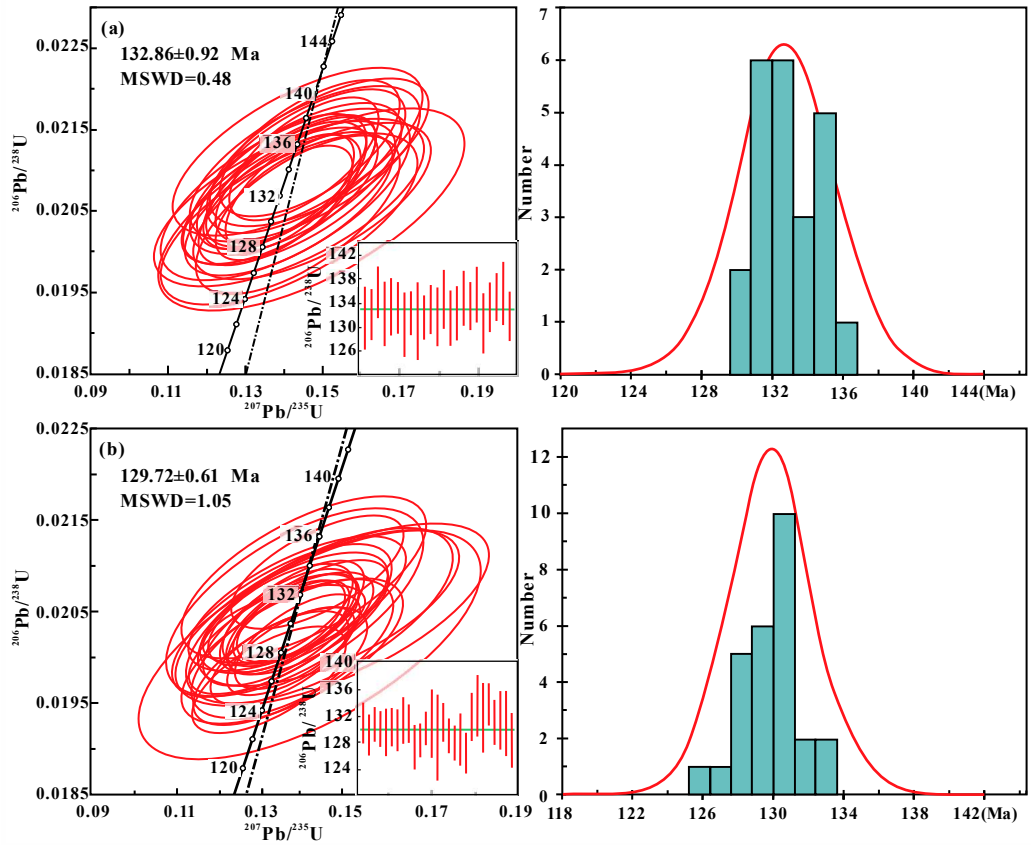

Figure 11. Zircon U-Pb concordia plots and weighted average ages for the Tietonggou pluton (**a**) and Laowa pluton (**b**). The error of isotope ratio and age is 2σ, and the confidence of weighted average age error is 95%.

5. Discussion

5.1. Age of Pluton

Early Cretaceous magmatic rocks are widely distributed in western Shandong, with most of the reported Ar-Ar ages clustered around 132–124 Ma [43,44]. Our study reports Early Cretaceous LA-ICP-MS zircon U-Pb ages of 132.86 ± 0.92 Ma (Tietonggou diorite) and 129.72 ± 0.61 Ma (Laowa diorite). It shows that both the Tietonggou diorite and the Laowa diorite were produced in the Cretaceous, which is consistent with the peak time of the lithospheric thinning of the North China Craton. Similar zircon U-Pb ages were also reported for the Mesozoic intrusive rocks (granitoids and gabbros) (132–122 Ma) in the eastern North China Craton (Jiaodong and Liaodong) [7,45,46]. This shows strong Early Cretaceous magmatic activity in the eastern part of the North China Craton.

5.2. Petrogenesis

The Tietonggou meladiorite and diorite are rich in MgO, Na_2O, Co, Ni, and other transitional elements, suggesting an upper mantle source [47]. The Nb/Ta value of the samples (14.27–16.82) is significantly higher than that of crust-derived magma (11.00) but basically consistent with that of mantle-derived magma (17.50) [48]. The Zr/Hf ratios (34.82–39.14) are close to the primitive mantle value (36.27) but much higher than the continental crust value (11.0) [34]. The samples also have Rb/Sr (0.10–0.16) and Ba/Rb (9.56–14.08) values close to the primitive mantle value (Rb/Sr = 0.03 [49], Ba/Rb = 11.00 [50]). The geochemical features of the Tietonggou pluton suggest a mantle-derived magma source. In the Ba/Rb-Rb/Sr diagram (Figure 12), the evolution trend of Tietonggou diorite samples is similar to that of the primitive mantle, suggesting that the rocks may have been mantle-sourced [51], consistent with the characteristics of compatible trace elements (e.g., Ni and Co). In addition, the Tietonggou pluton is rich in LILEs and depleted in HFSEs, giving a

Ta/La value (0.01–0.03) that is lower than the primitive mantle value (0.06) [52], indicating that crustal input must be considered in the petrogenesis. The Ce/Pb values of the samples (2.32–2.94, avg. 2.58) are significantly lower than those of MORB and OIB (25) but close to that of the upper crust (3.2), indicating significant crustal contamination in the magma evolution. Ratios of HFSEs and REEs can effectively identify the Cl-rich or F-rich ore-forming fluids: Cl-rich fluids commonly have LREEs enrichment and have Nb/La, Th/La, and Hf/Sm values < 1, whereas F-rich fluids have both LREE and HFSE enrichments and have Nb/La, Th/La, and Hf/Sm values > 1 [53]. For most Tietonggou samples, the Nb/La, Th/La, and Hf/Sm values are < 1, suggesting Cl-rich fluids (Table 1).

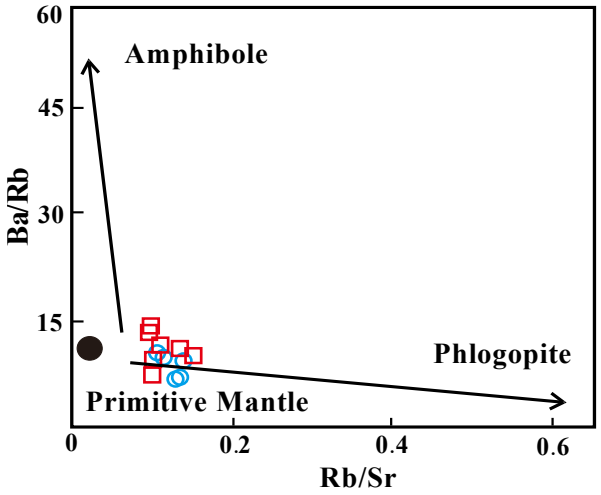

Figure 12. Ba/Rb vs. Rb/Sr plots for the Tietonggou meladiorite and diorite samples [51].

Pb isotope study [39] showed that Mesozoic mafic rocks in Eastern China have low initial radiogenic Pb isotope ratios, i.e., $^{206}Pb/^{204}Pb < 17.80$, $^{207}Pb/^{204}Pb < 15.00$, and $^{208}Pb/^{204}Pb < 38.00$, whereas those in the Yangtze Craton have high initial radiogenic Pb isotope ratios, i.e., $^{206}Pb/^{204}Pb > 17.80$, $^{207}Pb/^{204}Pb > 15.50$, and $^{208}Pb/^{204}Pb > 38.00$. The Tietonggou diorite has similar $^{206}Pb/^{204}Pb$ (>17.80) to those from the Yangtze Craton but similar $^{207}Pb/^{204}Pb$ (<15.50) and $^{208}Pb/^{204}Pb$ (<3800) to those from the NCC. This suggests that the magma formation was caused by the subduction of the Yangtze Plate beneath North China, so the magma source may be a mixture of the Yangtze and North China basement rocks (Table 2). For the study of intrusive rocks in the adjacent areas of western Shandong, the $^{207}Pb/^{204}Pb$ values of the Yinan gabbro in western Shandong are higher than those of the North China basic rocks, which may be modified by the subduction of the Yangtze craton [38]. Yang showed a spatial variation trend of Sr-Nd-Pb isotope of Early Cretaceous high-Mg diorite in western Shandong, of which $^{87}Sr/^{86}Sr$ and $^{207}Pb/^{204}Pb$ and $^{208}Pb/^{204}Pb$ decrease from southeast to northwest, whereas ε_{Nd} (t) increases [16,38]. This is consistent with the Yangtze plate subducted northwest beneath the North China Craton and the mixed Yangtze–North China magma source proposed for the Tietonggou pluton.

5.3. Tectonic Implications

The Tietonggou pluton emplacement is coeval with the earliest Cretaceous magmatism, which was the strongest Mesozoic magmatic event in the North China Craton and the whole of Eastern China [45,46,54–56]. During this time, large-scale magmatism, basin subsidence, and faulting occurred in the North China Craton, indicating strong lithospheric extension associated with the zenith of the North China decratonization [57,58]. Due to the subduction rollback, lithospheric delamination and asthenospheric upwelling occurred, forming extensive magmatism [59–62]. The formation of the Tietonggou pluton was closely related to this subduction event, and the magma was mainly sourced from the mantle. With the subduction of the Pacific plate to the North China plate, the asthenosphere upwelling

from deep (>150 km) to shallow caused decompression melting, the partial melting of the enriched lithospheric mantle, and the partial melting of mantle peridotite and subducted oceanic slab to produce basic magma.

6. Conclusions

(1) The western Shandong, located in the North China Craton, is one of the four major Fe–skarn deposit concentration areas in China, and the Tietonggou deposit is a representative deposit in this area. The study of the metallogenic age and source of ore-forming materials of the Tietonggou intrusion can contribute to the study of the Mesozoic magmatic evolution framework and the creation of the genetic model of Fe–skarn deposits in North China.

(2) Geochemical characteristics of the Tietonggou pluton and its inclusions suggest that the parental magma may have originated mainly from the enriched lithospheric mantle with minor continental crustal input. The magma formation was caused by the subduction of the Yangtze beneath North China, and the Tietonggou pluton was formed under the extension during the thinning of the lithosphere in this period.

(3) The view that the crustal input of metallogenic material in the Tietonggou deposit is derived from Archean North China or Paleo-Pacific materials could not be supported in this study.

(4) More research is needed to compare the genetic conclusions of the Tietonggou pluton with other Mesozoic plutons in western Shandong and to summarize the similarities in the geneses of these plutons.

Supplementary Materials: The following supporting information can be downloaded at: https://www.mdpi.com/article/10.3390/min14040390/s1, Table S1: Major oxides composition and trace elements composition for the Tietonggou diorite and meladiorite samples *.

Author Contributions: Conceptualization, G.M.; methodology, G.Y.; software, Y.H.; validation, H.Z.; formal analysis, G.Y.; investigation, Q.X. and Z.D.; resources, G.M.; data curation, G.Y; writing—original draft preparation, G.Y; writing—review and editing, G.Y.; visualization, Y.S.; supervision, Q.X. and Z.D.; project administration, G.M.; funding acquisition, G.M. All authors have read and agreed to the published version of the manuscript.

Funding: This research was funded by the National Natural Science Foundation of China (42172087, 41772125, 41572063), the Shandong Engineering Research Center of Application and Development of Big Data for Deep Gold Exploration (SDK202208), and the Major Scientific and Technological Innovation Projects of Shandong Province (2017CXGC1603).

Data Availability Statement: The data supporting this article are available in the online Supplementary Materials.

Acknowledgments: Thanks to the staff from the Institute of Geochemistry, the Chinese Academy of Sciences, the Beijing Zircon Navigation Technology Co., Ltd., and the State Key Laboratory of Continental Dynamics of Northwestern University for their support during the experiment. Special thanks are given to the three anonymous reviewers for their detailed and constructive reviews.

Conflicts of Interest: Yanchao Han, Huiji Zhao, and Ying Shen work for the Shandong Geo-surveying & Mapping Institute and Shandong Institute of Geological Sciences. The paper reflects the views of the scientists and not the institute.

References

1. Chen, Y.; Bin, S.U.; Guo, S. The Dabie-Sulu orogenic peridotites: Progress and key issues. *Sci. China Earth Sci.* **2015**, 1679–1699. [CrossRef]
2. Lan, T.G.; Fan, H.R.; Hu, F.F.; Tomkins, A.G.; Yang, K.F.; Liu, Y. Multiple crust–mantle interactions for the destruction of the North China Craton: Geochemical and Sr–Nd–Pb–Hf isotopic evidence from the Longbaoshan alkaline complex. *Lithos* **2011**, *122*, 87–106. [CrossRef]
3. Lan, T.G.; Fan, H.R.; Santosh, M.; Hu, F.F.; Yang, K.F.; Yang, Y.H.; Liu, Y. Early Jurassic high-K calc-alkaline and shoshonitic rocks from the Tongshi intrusive complex, eastern North China Craton: Implication for crust–mantle interaction and post-collisional magmatism. *Lithos* **2012**, *140–141*, 183–199. [CrossRef]

4. Li, S.R.; Santosh, M. Metallogeny and craton destruction: Records from the North China Craton. *Ore Geol. Rev.* **2014**, *56*, 376–414. [CrossRef]
5. Ma, Q.; Xu, Y.G.; Deng, Y.F.; Zheng, J.P.; Sun, M.; Griffin, W.L.; Xia, B.; Wang, C.Y. Similar crust beneath disrupted and intact cratons: Arguments against lower-crust delamination as a decratonization trigger. *Tectonophysics* **2019**, *750*, 1–8. [CrossRef]
6. Si, S.; Zheng, Y.; Liu, B.; Tian, X. Structure of the mantle transition zone beneath the North China Craton. *J. Asian Earth Sci.* **2016**, *116*, 69–80. [CrossRef]
7. Luo, Z.K.; Miao, L.C. *Granite and Gold Deposits in Zhaolai Area, Jiaodong*; Metallurgical Industry Press: Beijing, China, 2002. (In Chinese)
8. Wang, L.G.; Qiu, Y.M.; Mcnaughton, N.J.; Groves, D.I.; Liu, Y.K. Constraints on crustal evolution and gold metallogeny in the Northwestern Jiaodong Peninsula, China, from SHRIMP U–Pb zircon studies of granitoids. *Ore Geol. Rev.* **1998**, *13*, 275–291. [CrossRef]
9. Xu, W.L.; Wang, Q.H.; Wang, D.Y.; Pei, F.P.; Gao, S. Processes and mechanism of Mesozoic lithospheric thinning in eastern North China Craton: Evidence from Mesozoic igneous rocks and deep-seated xenoliths. *Earth Sci. Front.* **2004**, *1*, 309–317. (In Chinese)
10. Zhai, M.G.; Fan, Q.C.; Zhang, H.F.; Sui, J.L. Lower crust processes during the lithosphere thinning in eastern China: Magma underplating, replacement and delamination. *Acta Petrol. Sin.* **2005**, *21*, 1509–1526. (In Chinese)
11. Zhao, D.; You, T.; Lei, J.; Liu, L.; Zheng, S. Seismic image and origin of the Changbai intraplate volcano in East Asia: Role of big mantle wedge above the stagnant Pacific slab. *Phys. Earth Planet. Inter.* **2009**, *173*, 197–206. [CrossRef]
12. Yu, L.D.; Yu, X.F.; Li, D.P.; Liu, Q.; Liu, J.J.; Shu, L.; Wei, P.F. Zircon U–Pb Chronology, Geochemistry Characteristics of the Tiezhai Complex in Linqu County of Western Shandong and Their Geological Significance. *Geoscience* **2020**, *34*, 418–430. (In Chinese)
13. Ning, P.S.; Long, Q.; Cheng, T.; Hu, Z.P.; Cheng, F.K. Geochemistry and Sr–Nd–Pb Isotopic Composition of Late Mesozoic Intermediate-basic Rock in Western Shandong Block. *J. Earth Sci. Environ.* **2013**, *35*, 62–76. (In Chinese)
14. Wang, D.Y.; Xu, W.L.; Lan, X.; Wang, Q.H. Petrogenesis of pyroxenite xenoliths in Mesozoic gabbro-diorite from western Shandong Province, China. *J. Jilin Univ. Earth Sci. Ed.* **2004**, *34*, 167–173. (In Chinese)
15. Wu, X.Y.; Xu, Y.G.; Ma, J.L.; Xu, J.F.; Wang, Q. Geochemistry and petrogenesis of the Mesozoic high Mg diorites from western Shandong. *Geotecton. Et Metallog.* **2003**, *27*, 228–236. (In Chinese)
16. Yang, C.H.; Xu, W.L.; Yang, D.S.; Liu, C.C.; Liu, X.M.; Hu, Z.C. Petrogenesis of the Mesozoic High-Mg Diorites in West Shandong: Evidence from Chronology and Petro-geochemistry. *Earth Sci.* **2006**, *31*, 81–92. (In Chinese)
17. Yang, Q.L.; Zhao, Z.F.; Zheng, Y.F. Slab–mantle interaction in continental subduction channel: Geochemical evidence from Mesozoic gabbroic intrusives in southeastern North China. *Lithos* **2012**, *155*, 442–460. [CrossRef]
18. Yang, C.H. *Chronology and Geochemistry of Mesozoic High-Mg Diorites in Western Shandong: Constraints on Lithospheric Evolution of the North China Craton*; Jilin University: Jilin, China, 2007. (In Chinese)
19. Song, M.C.; Wang, P.C. *Regional Geology of Shandong Province*; Shandong Map Publishing House: Jinan, China, 2003. (In Chinese)
20. Dong, Z.X. *Yanshanian Intrusive Rocks and Mineralization in Central Shandong*; Geological Publishing House: Bath, UK, 1987. (In Chinese)
21. Zhou, Q.J. *Petrogenesis of Wehrlite and Pyroxenite Xenoliths in Early Cretaceous Igneous Rocks from Western Shandong, China*; Jilin University: Jilin, China, 2014. (In Chinese)
22. Xu, W.L.; Chi, X.G.; Yuan, C.; Huang, Y.M.; Wang, W. *Mesozoic Dioritic Rocks and Deep-Seated Inclusions in Central North China Platform*; Geological Publishing House: Beijing, China, 1993. (In Chinese)
23. Sannac, S.; Tadjiki, S.; Moldenhauer, E. Single particle analysis using the Agilent 7700x ICP-MS 2013. Available online: https://www.agilent.com/Library/applications/5991-2929EN.pdf (accessed on 2 April 2024).
24. Weis, D.; Kieffer, B.; Maerschalk, C.; Barling, J.; Jong, J.D.; Williams, G.A.; Scoates, J.S. High-precision isotopic characterization of USGS reference materials by TIMS and MC-ICP-MS. *Geochem. Geophys. Geosystems* **2006**, *7*, 139–149. [CrossRef]
25. Wiedenbeck, M.; Allé, P.; Corfu, F.; Griffin, W.L.; Meier, M.; Oberli, F.; Von Quadt, A.; Roddick, J.C.; Spiegel, W. Three natural zircon standards for U-Th-Pb, Lu-Hf, trace element and REE analyses. *Geostand. Newsl.* **1995**, *19*, 1–23. [CrossRef]
26. Wiedenbeck, M.; Hanchar, J.M.; Peck, W.H.; Sylvester, P.; Valley, J.; Whitehouse, M.; Kronz, A.; Morishita, Y.; Nasdala, L.; Fiebig, J.; et al. FurtherCharacterisation of the 91500 Zircon Crystal. *Geostand. Geoanalytical Res.* **2004**, *28*, 9–39. [CrossRef]
27. Jackson, S.E.; Pearson, N.J.; Griffin, W.L. The applcation of laser ablation-inductively coupled plasma-mass spectrometry to in situ U-Pb zircon geochronology. *Chem. Geol.* **2004**, *211*, 47–69. [CrossRef]
28. Yuan, H.L.; Gao, S.; Liu, X.M.; Li, H.M.; Detlef, G.; Wu, F.Y. Accurate U-Pb Age and Trace Element Determinations of Zircon by Laser Ablation-Inductively Coupled Plasma-Mass Spectrometry. *Geostand. Geoanalytical Res.* **2007**, *28*, 353–370. [CrossRef]
29. Middlemost, E. Naming materials in the magma/igneous rock system. *Earth-Sci. Rev.* **1994**, *37*, 215–224. [CrossRef]
30. Irvine, T.N.; Baragar, W.R.A. A Guide to the Chemical Classification of the Common Volcanic Rocks. *Can. J. Earth Sci.* **1971**, *8*, 523–548. [CrossRef]
31. Papu, D.M.; Philip, M.P. Tectonic discrimination of granitoids. *Geol. Soc. Am. Bull.* **1989**, *101*, 635–643.
32. Wright, J.B. A simple alkalinity ratio and its application to questions of non-orogenic granite genesis. *Geol. Mag.* **1969**, *106*, 370–384. [CrossRef]
33. Kelemen, P.B.; Shimizu, N.; Dunn, T. Relative depletion of niobium in some arc magmas and the continental crust: Partitioning of K, Nb, La and Ce during melt/rock reaction in the upper mantle. *Earth Planet. Sci. Lett.* **1993**, *120*, 111–134. [CrossRef]

34. Liu, Y.J.; Liu, B.Q.; Feng, Z.Q.; Wen, Q.B.; Li, W.M.; Zhang, T.A.; Du, B.Y. SIMS Zircon U–Pb Age, Petrogeochemistry and Its Tectonic Implication of Laodaokou Diorite in the Mid-North Part of Great Xing'an Range. *J. Jilin Univ. Earth Sci. Ed.* **2016**, *46*, 482–498. (In Chinese)
35. Boynton, W.V. Geochemistry of the rare earth elements: Meteorite studies. In *Rare Earth Element Geochemistry 2*; Elsevier: Amsterdam, The Netherlands, 1984.
36. Taylor, S.R.; McLennan, S.M. *The Continental Crust: Its Composition and Evolution*; Blackwell: Hoboken, NJ, USA, 1985.
37. Yang, C.H.; Xu, W.L.; Yang, D.S.; Wang, W.; Wang, W.D.; Liu, J.M. Petrogenesis of shangyu gabbro-diorites in western shandong: Geochronological and geochemical evidence. *Sci. China Ser. D Earth Sci.* **2008**, *51*, 481–492. [CrossRef]
38. Li, S.G.; Yang, W. Decoupling of surface and subsurface sutures in the Dabie orogen and a continent-collisional lithospheric-wedging model: Sr-Nd-Pb isotopic evidences of Mesozoic igneous rocks in eastern China. *Chin. Sci. Bull.* **2003**, *48*, 831–838. [CrossRef]
39. Yan, J.; Cheng, J.F.; Yu, G.; Qian, H.; Zhou, T.X. Pb Isotopic Characteristics of Late Mesozoic Mafic Rocks from the Lower Yangtze Region: Evidence for Enriched Mantle. *Geol. J. China Univ.* **2003**, *9*, 195–206. (In Chinese)
40. Yang, D.B.; Xu, W.L.; Pei, F.P.; Yang, C.H.; Wang, Q.H. Spatial extent of the influence of the deeply subducted South China Block on the southeastern North China Block: Constraints from Sr–Nd–Pb isotopes in Mesozoic mafic igneous rocks. *Lithos* **2012**, *136–139*, 246–260. [CrossRef]
41. Stanley, R.H. A large-scale isotope anomaly in the Southern Hemisphere mantle. *Nature* **1984**, *309*, 753–757.
42. Hu, F.F.; Fan, H.R.; Yang, J.H.; Wan, Y.S.; Liu, D.; Zhai, M.G.; Jin, C.W. Metallogenic age of gold bearing quartz vein type gold deposit in Rushan, Eastern Shandong: U–Pb determination by hydrothermal zircon SHRIMP method. *Chin. Sci. Bull.* **2004**, *49*, 1191–1198. (In Chinese)
43. Wang, S.J.; Zhang, C.J.; Yang, E.X.; Song, Z.Y.; Wang, L.F.; Xu, K.M. Division of Mesozoic Intrusive Stages in Luxi Area. *Shandong Land Resour.* **2009**, *25*, 18–23. (In Chinese)
44. Xu, W.L.; Wang, D.Y.; Wang, Q.H.; Pei, F.P.; Lin, J.Q. 40Ar/39Ar dating of hornblende and biotite in Mesozoic intrusive complex from the North China Block: Constraints on the time of lithospheric thinning. *Geochimica* **2004**, *33*, 221–231. (In Chinese)
45. Wu, F.Y.; Lin, J.Q.; Wilde, S.A.; Zhang, X.; Yang, J.H. Nature and significance of the Early Cretaceous giant igneous event in eastern China. *Earth Planet. Sci. Lett.* **2005**, *233*, 103–119. [CrossRef]
46. Yang, D.B.; Xu, W.L.; Pei, F.P.; Wang, Q.H.; Gao, S. Chronology and Pb isotope compositions of Early Cretaceous adakitic rocks in Xuzhou-Huaibei area, central China: Constraints on magma sources and tectonic evolution in the eastern North China Craton. *Acta Petrol. Sin.* **2008**, *24*, 1745–1758. (In Chinese)
47. Rapp, R.P.; Watson, E.B. Dehydration Melting of Metabasalt at 8–32 kbar: Implications for Continental Growth and Crust-Mantle Recycling. *J. Petrol.* **1995**, *36*, 891–931. [CrossRef]
48. Green, T.H. Significance of Nb/Ta as an indicator of geochemical processes in the crust-mantle system. *Chem. Geol.* **1995**, *120*, 347–359. [CrossRef]
49. Ionov, D.A.; Griffin, W.L.; O'Reilly, S.Y. Volatile-bearing minerals and lithophile trace elements in the upper mantle. *Chem. Geol.* **1997**, *141*, 153–184. [CrossRef]
50. McDonough, W.F.; Sun, S.S. The composition of the Earth. *Chem. Geol.* **1995**, *120*, 223–253. [CrossRef]
51. Zhang, C.; Cui, F.H.; Zhang, Z.L.; Geng, R.; Song, M.C. Petrogenesis of Ore-Bearing Dioritic Pluton in Jinling Area in Western-Shandong: Evidence from Zircon U-Pb Chronology and Petro-Geochemistry. *J. Jilin Univ. Earth Sci.* **2017**, *47*, 1732–1745.
52. Wood, D.A.; Tarney, J.; Varet, J.; Saunders, A.D.; Cann, J.R. Geochemistry of basalts drilled in the North Atlantic by IPOD Leg 49: Implications for mantle heterogeneity. *Earth Planet. Sci. Lett.* **1979**, *42*, 77–97. [CrossRef]
53. Oreskes, N.; Einaudi, M.T. Origin of rare earth element-enriched hematite breccias at the Olympic Dam Cu-U-Au-Ag deposit, Roxby Downs, South Australia. *Econ. Geol.* **1990**, *85*, 1–28. [CrossRef]
54. Wang, D.Z.; Zhou, X.M. *Genesis and Crustal Evolution of Late Mesozoic Granitic Volcanic Intrusive Complexes in Southeastern China*; Science Press: Beijing, China, 2002. (In Chinese)
55. Wu, F.Y.; Han, R.H.; Yang, J.H.; Wilde, S.A.; Zhai, M.G.; Park, S.C. Initial constraints on the timing of granitic magmatism in North Korea using U–Pb zircon geochronology. *Chem. Geol.* **2007**, *238*, 232–248. [CrossRef]
56. Xu, Y.G.; Huang, X.L.; Ma, J.L. Crust-mantle interaction during the tectono-thermal reactivation of the North China Craton: Constraints from SHRIMP zircon U–Pb chronology and geochemistry of Mesozoic plutons from western Shandong. *Contrib. Mineral. Petrol.* **2004**, *147*, 750–767. [CrossRef]
57. Zhu, R.X.; Chen, L.; Wu, F.Y.; Liu, J.L. Timing, scale and mechanism of the destruction of the North China Craton. *Sci. China Earth Sci.* **2011**, *54*, 789–797. [CrossRef]
58. Zhu, R.X.; Xu, Y.G. Subduction of the Western Pacific plate and destruction of the North China Craton. *Sci. China Earth Sci.* **2019**, *62*, 1340–1350. [CrossRef]
59. Goss, S.C.; Wilde, S.A.; Wu, F.; Yang, J. The age, isotopic signature and significance of the youngest Mesozoic granitoids in the Jiaodong Terrane, Shandong Province, North China Craton. *Lithos* **2010**, *120*, 309–326. [CrossRef]
60. Yang, Q.Y.; Santosh, M. Early Cretaceous magma flare-up its implications on gold mineralization in the Jiaodong Peninsula, China. *Ore Geol. Rev.* **2015**, *65*, 626–642. [CrossRef]

61. Deng, C.Z.; Gou, J.; Sun, D.Y.; Sun, G.Y.; Tian, Z.D.; Lehmann, B.; Moynier, F.; Yin, R.S. Mercury isotopic composition of igneous rocks from an accretionary orogen: Implications for lithospheric recycling. *Geology* **2022**, *50*, 1001–1006. [CrossRef]
62. Deng, C.Z.; Fu, A.Z.; Geng, H.Y.; Sun, D.Y.; Zhao, G.C.; Mao, G.Z.; Moynier, F.; Lehmann, B.; Yin, R.S. Low-$\delta^{18}O$ and negative $\Delta^{199}Hg$ felsic igneous rocks in NE China: Implications for Early Cretaceous orogenic thinning. *Chem. Geol.* **2023**, *633*, 121569. [CrossRef]